Supporting Information: Quantitative dielectrophoretic tracking for characterization and separation of persistent subpopulations of *Cryptosporidium parvum*

S1. Quantifying DEP force on the oocysts from velocity tracking measurements: For a particle accelerated under a dielectrophoretic force (F_{DEP}), based on Netwon's second law, the net force on the particle of radius: a, within a medium of viscosity: η, can be determined by tracking displacement (x) as a function of time (t):

$$F_{DEP} - 6\pi\eta a\frac{dx}{dt} = m\frac{d^2x}{dt^2} \ldots Eq.(S1)$$

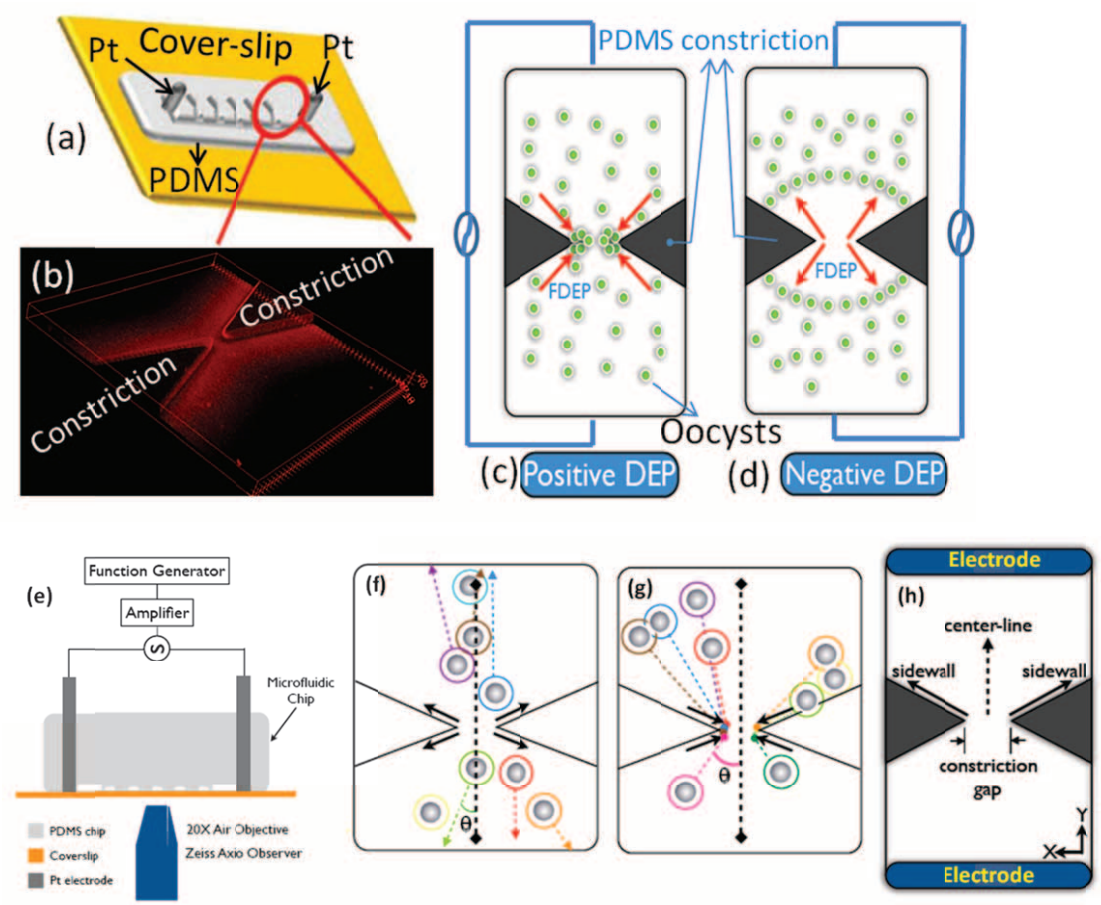

Figure S1: (a) Schematic device; (b) confocal image of constriction chip; and force directions under: (c) positive DEP (PDEP), and: (d) negative DEP (NDEP). (e) Set-up for observing DEP behavior of oocysts. Translation vectors for oocysts under: (f) NDEP; and (g) PDEP. (h) Center-line and sidewall vectors for the constriction device. The angle θ measured for the oocyst displacement is measured with regards to the device axis or center-line, as per (f) and (g).

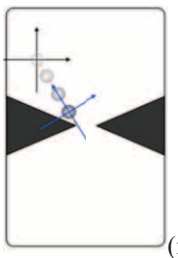

(i)

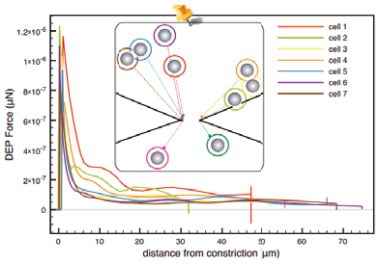

(j)

Figure S1:
(i) Coordinate Transformation
(j) Typical force profiles in pN versus distance from constriction tip for untreated oocysts. There are ~25-30 data points over the constriction region and force profiles peak at 2-4 μm from constriction tip. This peak force is reported in Figure 6A.

Coordinate transformation for displacement versus time tracking: The set-up for imaging the dielectrophoretic translation of oocysts is shown in Figure S1a and S1e. Based on data from high frame per second (~30 fps) movies of oocyst translation under F_{DEP}, the displacement (x) is tracked as a function of time (t) for particles translated away from the constriction tip under negative DEP (NDEP) and towards the constriction tip under positive DEP (PDEP). For NDEP, the translation of oocysts that were originally at rest at the constriction tip prior to application of AC field at the particular frequency of interest is recorded as displacement versus time of field, onwards from the constriction tip along a particular displacement vector (Figure S1f). For PDEP, the translation of oocysts that were originally at rest in the region immediately outside of the constriction gradient prior to application of AC field at the particular frequency of interest is recorded as displacement versus time of the field, towards the constriction tip along a particular displacement vector (Figure S1g). While the measurements are done in two dimensional space, we can cut down the computations for the force calculations by half by performing the following coordinate transformation. Since the cells always move in a straight line, either towards or away from the constriction tip, for the duration that they are acted upon by DEP, hence, we can track their translation along a particular displacement vector and change our frame of reference so that their motion takes place only in one of the two axes. In order to accomplish this, the coordinate system in which the motion is recorded must be transformed from the standard to a system that has been rotated by an angle that is equal to the angle that the oocyst's trajectory makes with the centerline, along the device axis (Figure S1(i)). Note that the angle of rotation must always be measured in the counter-clockwise direction from an axis of the standard coordinate system to the corresponding axis of the new system. This transform renders one of the dimensions unnecessary, thereby enabling the computation of the force in one-dimensional space. In this manner, the experimental raw data acquired in the form of video, is processed to yield a table of position versus time; i.e. (x,y,t) coordinates for the analyzed oocysts and then transformed into a linear (y,t) set by using the following coordinate transformation:

$$x' = x\cos\theta - y\sin\theta; y' = x\sin\theta + y\cos\theta \ldots Eq.(S2)$$

The modified displacement data as a function of time is algorithmically smoothed by using a high-order polynomial fit, since the faster displacements under higher F_{DEP} require higher frame rates for accurately tracking displacement over time, versus the slower displacements. Furthermore, while the oocyst is several pixels large in the video images, the tracking only records one central pixel per frame, which leads to some degree of noise in the data, which can be smoothed out using the polynomial fit. Hence, having a larger number of displacement versus time points, as obtained with the field non-unifoprmity of enhanced spatial extent for the constriction device improves the accuracy of the computed DEP force data. To ensure an effective smoothing, we check for the lack of jagged features on the derivatives of Eq. (S1). As a result we obtain (dx/dt) and (d^2x/dt^2) for the oocysts at a particular applied field and frequency, after each of the disinfection treatments, which can be used to compute the F_{DEP} frequency response in the direction of the particle trajectory ("track" direction).

Normalizing for field non-uniformities: Within the constriction device, the profile of the electric field and hence, F_{DEP}, varies depending on the displacement vector of the oocysts. This can create a variation in F_{DEP} of up to an order of magnitude, depending on displacement direction and distance of the oocysts in relationship to the constriction tip of a given device. Hence, we normalized all the data for field differences from the velocity tracked direction (track) to that

along the centerline direction (CL), by accounting for the field differences (∇E^2) between the "track" and "centerline" directions through a normalization factor: $K = \frac{\nabla E^2_{track}}{\nabla E^2_{CL}}$; $F^{CL}_{DEP} = \frac{F^{track}_{DEP}}{K}$

The ∇E^2 in the "track" direction is calculated by translating the measured trajectory of the oocyst to a simulation of the device in order to read the magnitude and gradient of the electric field along this vector direction. The magnitude and gradient of the electric field along the centerline direction is also available from this simulation. In this manner, by dividing the computed DEP force along the "track" direction by the field enhancement ratio K, we ensure that all the variations in DEP force can be solely attributed to variations in particle polarizability, rather than field non-uniformities due to the device device geometry. A typical set of force profile data for untreated oocysts is shown in Figure S1(j).

S2. Computing of dielectric parameters by fitting the DEP frequency response: The measured F_{DEP} versus frequency response of was fit to a single shell model [1, 2]. The model assigns different electrical properties to the core (cytoplasm) and the shell (membrane) of the oocyst. The Maxwell-Wagner interfacial polarization is then calculated at the interface between each level of the shells. The total polarization is described by the compound Clausius-Mossotti factor (K_{CM}) from all the shells, which can be determine from the measured DEP force as:

$$K_{CM} = \frac{\mathbf{F}_{DEP}}{2\pi a^3 \varepsilon_m \nabla E^2} \ldots Eq.(S3)$$

Here, ∇E^2 can be determined from finite element simulations of the electric field (E) and its gradient (∇E) across the device. ε_m is the medium permittivity and *a* is the radius of the oocyst. As per Figure S2, based on a medium permittivity: ε_1; shell permittivity of ε_2 and cytoplasm permittivity of ε_3, a net particle permittivity can be written as ε_{23}. The K_{CM} is given by the respective complex permittivity values, as follows:

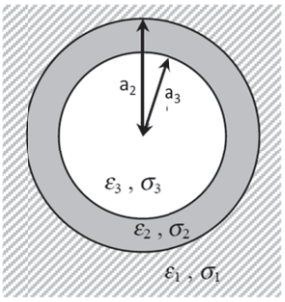

Figure S2: Dielectric parameters for shell model [2].

$$K_{CM} = \frac{\varepsilon^*_{23} - \varepsilon^*_1}{\varepsilon^*_{23} + 2\varepsilon^*_1} \ldots Eq.(S4)$$

ε_{23}* can be calculated from K_{CM} as follows:

$$\varepsilon^*_{23} = \varepsilon_1 \frac{2K_{CM}+1}{1-K} \ldots Eq.\ (S5)$$

To calculate the dielectric properties of the shell: ε_2, σ_2; and the cytoplasm: ε_3, σ_3, for a shell to cytoplasm radius ratio of: $\gamma = a_2/a_3$, ε_{23}* is used as follows:

$$\varepsilon^*_{23} = \frac{\varepsilon^*_2(\gamma^3 + 2\left(\frac{\varepsilon^*_3 - \varepsilon^*_2}{\varepsilon^*_3 + 2\varepsilon^*_2}\right))}{\gamma^3 - \left(\frac{\varepsilon^*_3 - \varepsilon^*_2}{\varepsilon^*_3 + 2\varepsilon^*_2}\right)} \ldots Eq.\ (S6)$$

Note, that the complex permittivity valuees can be related to conductivity and permittivity, as follows:

$$\varepsilon^*_2 = \varepsilon_2 + \frac{\sigma_2}{j\omega};\ \varepsilon^*_3 = \varepsilon_3 + \frac{\sigma_3}{j\omega} \ldots Eq.\ (S7)$$

Upon substituting these equations, the dielectric parameters of the shell and core can be calculated from ε_{23}*, as follows:

$$\varepsilon_{23}^{*} = \frac{(\varepsilon_2 + \frac{\sigma_2}{j\omega})\,(\gamma^3 + 2\left(\frac{(\varepsilon_3 - \varepsilon_2) + \frac{j}{\omega}(\sigma_2 - \sigma_3)}{(\varepsilon_3 + 2\varepsilon_2) - \frac{j}{\omega}(\sigma_3 + 2\sigma_2)}\right))}{\gamma^3 - \left(\frac{(\varepsilon_3 - \varepsilon_2) + \frac{j}{\omega}(\sigma_2 - \sigma_3)}{(\varepsilon_3 + 2\varepsilon_2) - \frac{j}{\omega}(\sigma_3 + 2\sigma_2)}\right)} \ldots Eq.(S8)$$

A numerical non-linear least square fitting algorithm was then used to calculate the unknown permittivity and conductivity parameters. Multiple runs were performed, each with different starting points to ensure that the optimized solutions converge to a global minimum.

S3. Morphological modifications to *Cryptosporidium parvum* after disinfectant treatments:

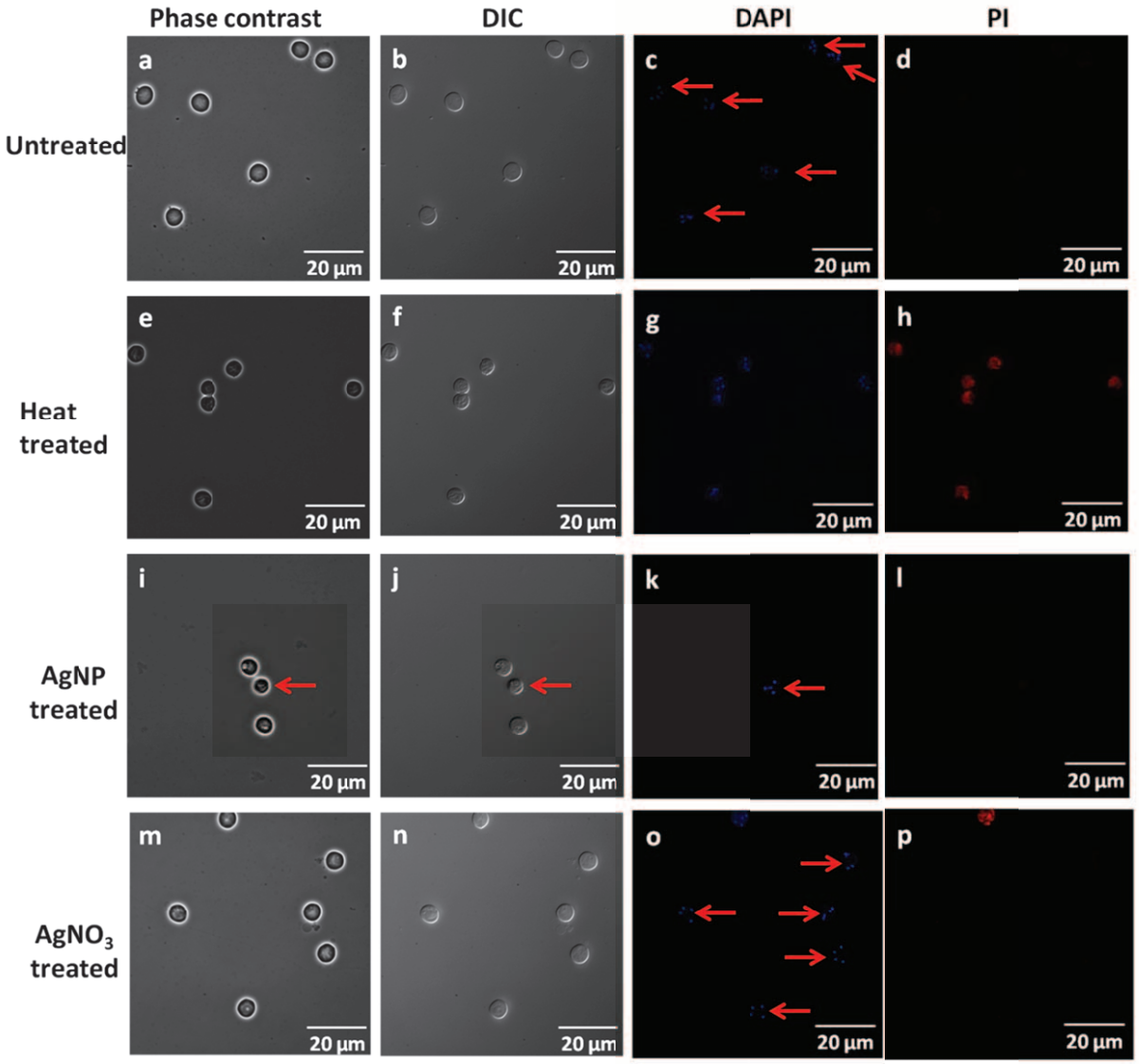

Figure S3: Optical microscopy of oocysts after various treatments, as measured by various imaging modes within the same field of view: Column 1: phase contrast; Column 2: Nomarski Differential Interference Contrast (DIC); Column 3: DAPI fluorescence; Column 4: PI fluorescence; for: untreated (a

– d); heat-treated (e – h); AgNP treated (i – l); $AgNO_3$ treated (m – p) oocysts. Arrows indicate DAPI inclusion and PI exclusion.

The manuscript describes the alterations of *Cryptosporidium parvum* oocysts under high resolution phase contrast and Nomarski differential interference contrast (DIC) microscopy before and after disinfectant treatments, including heat, AgNP and $AgNO_3$ treatments. Briefly, phase contrast microscopy of untreated oocysts using a high resolution phase objective and camera reveals the transparent oocyst wall and four intact sporozoites arranged in a banana-shape, as apparent in **Figure 2a**. The DIC image of the untreated oocysts in **Figure 2b** provides topographic evidence for the presence of intact sporozoites [3]. Upon heat treatment, instead of the distinct banana-shaped arrangement of the sporozoites, the oocyst cytoplasm is filled with nebulous undistinguishable structures, as apparent in the phase contrast image (**Figure 2e),** while the DIC image also reveals a disorganized sporozoite structure in the oocyst (**Figure 2f**). Following treatment with AgNPs, the banana-shaped arrangement of the sporozoites is no longer detectable, within some oocysts indicated as: Sp ×. Instead, the oocyst cytoplasm in **Figure 2i** reveals a coalesced cluster that seems transparent in the phase contrast image adjoining an empty region, suggesting an altered sporozoite structure. The DIC image (**Figure 2j)** shows the smooth surface of the big cluster, with a clear topographic difference between the cluster and the empty region. However, there is a small group of the AgNP treated oocysts that continue to show the sporozoite morphology of untreated oocysts, as indicated by: Sp √. Since the phase and DIC images within Figure 2 of the manuscript are at higher magnification than that of the fluorescence images, the field of view of the images were altered. To enable a clearer comparison of the phase and DIC images with the fluorescence images, Figure S3 shows the respective modes at the same magnification and field of view. The correlation of sporozoite structure from the phase and DIC images to their fluorescence is apparent for oocysts within the same field of view in Figure S3.

S4. Heterogeneous alterations to the oocyst wall after heat treatment at 70°C:

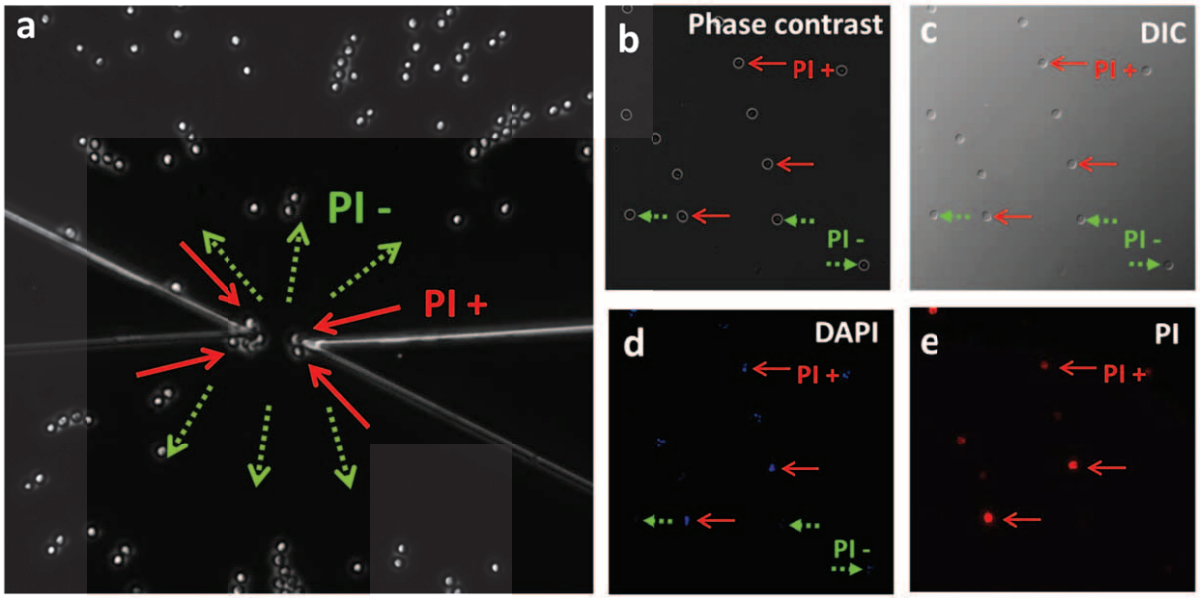

Figure S4: Dielectrophoretic separation of oocysts based on oocyst wall condition after heat treatment at 70°C for 5 minutes: (a) PDEP behavior of oocysts with permeable oocyst walls (PI +) versus NDEP behavior of oocysts with less permeable oocyst walls (PI -). (b) Phase contrast; (c) DIC; (d) DAPI; and (e) PI images confirm the presence of the sub-groups with fully-disrupted and partially disrupted oocysts walls.

Heat treatment of the oocysts at 70°C for 5 minutes caused a heterogeneous sample of oocysts with varying degrees of permeability of the oocyst wall. The separation of these oocysts based on permeability of the oocyst wall was described in Figure 4h – 4j of the manuscript. Figure S4 shows additional evidence for the heterogeneous alterations to the oocyst wall after this particular treatment. Under fields at 100 kHz, as per Figure S4a, oocysts with uncompromised walls exhibit NDEP behavior (green dotted arrows) and those with disrupted walls exhibit PDEP behavior (red solid arrows). The presence of the two sub-groups is also confirmed by the presence of DAPI (**Figure S4d**) and PI (**Figure S4e**) signals in one group (red solid arrows), with the other group showing the presence of faint DAPI signal (green dotted arrows in **Figure S4d**) and the absence of PI signal (**Figure S4e**) in the same field of view. The phase contrast (Figure S4b) and DIC (Figure S4c) images of the same field of view confirm morphological differences in the oocyst wall for the two sub-groups.

S5. Crossover frequency method: The crossover frequency can be determined for varying media conductivity, as shown in Figure S5. Using notation from S2:

$$\tilde{\epsilon_{23}} = \tilde{\epsilon_1} \cdot \frac{2K+1}{1-K}$$

Setting $K = 0$, we find that:

$$\tilde{\epsilon_{23}} = \tilde{\epsilon_1}$$

Since we know $\tilde{\epsilon_1}$ from the experiments, we now know what $\tilde{\epsilon_{23}}$ should be.
Again, according to the shell model,

$$\tilde{\epsilon}_{23} = \frac{\tilde{\epsilon}_2\left(\gamma^3 + 2\frac{\tilde{\epsilon}_3 - \tilde{\epsilon}_2}{\tilde{\epsilon}_3 + 2\tilde{\epsilon}_2}\right)}{\left(\gamma^3 - \frac{\tilde{\epsilon}_3 - \tilde{\epsilon}_2}{\tilde{\epsilon}_3 + 2\tilde{\epsilon}_2}\right)} = \tilde{\epsilon}_1$$

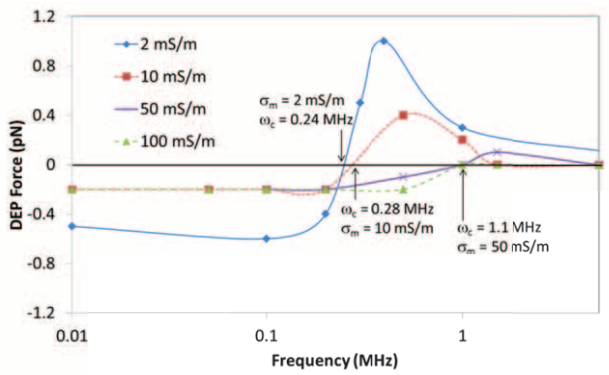

Figure S5: ω_c for untreated oocysts at different σ_m.

By setting the Clausius Mossoti factor to be zero at ω_c, we can determine the dielectric properties as follows, using a non-linear least-squares fitting routine:

Method	σ_{wall} (S/m)	ε_{wall}	σ_{cyto} (S/m)	ε_{cyto}
ω_c	1 x 10^{-8}	10	0.06	50
F_{DEP}	6 x 10^{-7}	8	0.055	55

This demonstrates that our method based on F_{DEP} tracking agrees with the crossover frequency method (at ω_c) without the need to rely on DEP measurements over multiple media conductivities (σ_m).

References

[1] T. B. Jones, Electromechanics of Particles, Cambridge, New York: Cambridge University Press, 1995
[2] H. Morgan and N. G. Green, AC Electrokinetics: Colloids and Nanoparticles, Williston, VT, USA: Research Studies Press Ltd., 2003.
[3] L. J. Anguish and W. C. Ghiorse, "Computer-Assisted Laser Scanning and Video Microscopy for Analysis of Cryptosporidium parvum Oocysts in Soil, Sediment, and Feces," *Appl Environ Microbiol,* vol. 63, pp. 724-33, Feb 1997.